



Oxygen transport in zeolite Y measured by quenching of encapsulated tris(bipyridyl)ruthenium

Michael A. Coutant, Pramatha Payra, Prabir K. Dutta *

Department of Chemistry, The Ohio State University, 100 West 18th Avenue, Columbus, OH 43210, USA

Received 22 December 2002; accepted 3 March 2003

Abstract

This study deals with emission quenching of zeolite encapsulated trisbipyridyl ruthenium (II) ($\text{Ru}(\text{bpy})_3^{2+}$) by oxygen. Oxygen saturated solutions of $\text{Ru}(\text{bpy})_3^{2+}$ typically show about 70% quenching ($I_0/I = 3.3$), where I_0 and I are the peak intensities of the emission in N_2 and O_2 , respectively. However, an aqueous suspension of $\text{Ru}(\text{bpy})_3^{2+}$ -zeolite Na–Y (Si/Al = 2.5) (abbreviated as Ru–Na–Y) showed no quenching at all. This observation motivated us to analyze how the transport of O_2 is occurring in the zeolite. Upon exposure of solid Ru–Na–Y (99% of intrazeolitic water) to N_2/O_2 dry gases, quenching in oxygen was found to be 5% ($I_0/I = 1.07$). Partial dehydration at room temperature with loss of 33% of the water molecules from the zeolite led to 66% ($I_0/I = 2.96$) quenching. Dehydration of Ru–Na–Y at 250 °C under vacuum overnight led to complete loss of intrazeolitic water and increased quenching to 90% ($I_0/I = 10.7$). Nanocrystalline $\text{Ru}(\text{bpy})_3^{2+}$ -zeolite Y upon vacuum dehydration lost 55% of the intrazeolitic water and showed 96% ($I_0/I = 25.3$) quenching. The extent of quenching of $\text{Ru}(\text{bpy})_3^{2+}$ in zeolites by O_2 is by far the largest as compared to previously studied matrices, and is being attributed to confinement of O_2 in the supercages, which leads to increase in number of collisions with $\text{Ru}(\text{bpy})_3^{2+}$ and enhanced quenching. However, these samples showed complete lack of sensitivity ($I_0/I = 1$) to oxygen upon exposure to water saturated gas or dissolved gas. Dealumination of zeolite framework by treatment with $(\text{NH}_4)_2\text{SiF}_6$ produced a framework of Si/Al = 9.5, and with SiCl_4 a framework of Si/Al > 100. With increasing dealumination, the extent of quenching by dissolved O_2 increased.

© 2003 Elsevier Science Inc. All rights reserved.

Keywords: Oxygen sensor; Zeolite diffusion; Zeolite confinement

1. Introduction

The microporous nature of zeolites is extensively exploited for catalytic hydrocarbon trans-

formations and gas separations [1]. In these processes, the ability of gas phase molecules to diffuse through the zeolitic pores is critical. For this reason, there has been considerable interest in understanding the nature of intrazeolitic gas diffusion [2]. Common methods for the measurement of intrazeolitic diffusion include pulsed field gradient NMR spectroscopy, gas chromatography and gravimetric measurements and are done with dehydrated zeolites [3]. Recently, the organized

* Corresponding author. Tel.: +1-614-292-4532; fax: +1-614-688-5402.

E-mail address: dutta.1@osu.edu (P.K. Dutta).

architecture of zeolites is being exploited for novel applications involving photochemistry, electrochemistry and as sensors [4]. Migration of small molecules within zeolites is relevant for these applications.

In this study, we focus on understanding the migration of O₂ within zeolites using the emission quenching of zeolite encapsulated ruthenium trisbipyridyl [Ru(bpy)₃²⁺] as the probe. Oxygen is known to be an efficient quencher of photoexcited Ru(bpy)₃²⁺ by an energy transfer process. The resulting deactivation of the luminescent state, Ru(bpy)₃²⁺ allows for spectroscopic monitoring of the interaction with oxygen by measuring either emission intensity or excited-state lifetime [5]. Studies of [Ru(bpy)₃²⁺] synthesized within the supercages of zeolite Y (abbreviated henceforth as Ru–Na–Y) have shown that once synthesized, the ruthenium complex is permanently entrapped [6], but readily available for electron transfer quenching by a wide variety of electron acceptors [7]. Since the ability of oxygen to quench Ru(bpy)₃²⁺ is determined by its access to the intrazeolitic ruthenium complex, the quenching characteristics provide information on the migration of oxygen molecules through the zeolite framework.

Wolfbeis and co-workers have exploited this encapsulation technique for making optical oxygen sensors [8]. Their investigation focused on the gas phase sensing properties of Ru(bpy)₃²⁺-Y dispersed within a silicone polymer.

In the present study, insight into O₂ transport was gained through measurement of the magnitude of oxygen quenching and analysis of the Stern–Volmer plots. The quenching was studied as a function of several variables related to the zeolite, including water content, Tl exchange, nanocrystalline and dealuminated zeolites. Modifications to the zeolite that resulted in a decrease in water content proved effective in promoting quenching. The efficiency of quenching of intrazeolitic Ru(bpy)₃²⁺ was considerably higher than previously reported studies of Ru(bpy)₃²⁺ supported on other solid matrices by almost an order of magnitude. Quenching by oxygen dissolved in water was only observed with dealuminated zeolites, the efficiency increasing with dealumination.

2. Experimental

2.1. Synthesis of zeolite nanocrystals

The method of preparation of nanocrystalline zeolite Y was adapted from the procedure of Otterstedt et al. [9]. A tetramethylammonium-aluminate solution was made by dissolving Al₂(SO₄)₃ · 18H₂O (J.T. Baker) in distilled water. Aluminum hydroxide was precipitated by adding excess NH₄OH (Mallinkrodt). The Al(OH)₃ was repeatedly washed with distilled water until all sulfate ions have been removed. The final slurry of Al(OH)₃ and water was then dissolved in a tetramethylammonium (TMA) hydroxide (Sachem, Inc.). A small amount of NaOH (Mallinkrodt) was added and the mixture was shaken to produce a clear solution. With strong mixing, the TMA-aluminate solution was added to tetraethylorthosilicate (Aldrich) resulting in a clear mixture. The final molar composition of the solution was: 2.5(TMA)₂O:0.05Na₂O:1.0Al₂O₃:3.4SiO₂:370H₂O. The final solution was placed in a Teflon bottle, capped and heated at 100 °C for 3 days and the zeolite isolated using an ultracentrifuge (20,000 rpm) and washed several times with distilled water and 1 M NaCl (Fisher).

2.2. Dealumination of zeolite framework

Dealumination of the Ru–Y with (NH₄)₂SiF₆ (Aldrich) followed the procedure of Skeels et al. [10]. 125 mg of NH₄⁺ exchanged Ru–Y was placed in a flask containing 10 ml of 0.8 M ammonium acetate (Jenneile Chem. Co.) solution. The solution was heated to 80 °C and to this solution 10 ml of 0.067 M (NH₄)₂SiF₆ was added dropwise (4–5 drops/min) with stirring. The mixture was kept at 80 °C with stirring for 3 h. The final solution was filtered and washed several times with distilled water. Samples with Si/Al > 100 were made by the treatment of Na–Y (Si/Al = 2.5) with SiCl₄ vapor at 500 °C [11].

2.3. Zeolite ion exchange

Ion exchange was performed by stirring 200 mg of zeolite overnight in 1 M solutions of a saturated TiNO₃ (Alfa Products) solution.

2.4. $Ru(bpy)_3^{2+}$ -Y synthesis (Ru–Na–Y)

$Ru(bpy)_3^{2+}$ was synthesized in zeolite Na–Y (Si/Al = 2.5) by conventional ship-in-a-bottle synthesis, at a loading level of 1 molecule of $Ru(bpy)_3^{2+}$ per 15 zeolite supercages [6]. The solid exhibited the characteristic metal-to-ligand charge transfer absorption band of $Ru(bpy)_3^{2+}$ at ~ 450 nm and the corresponding emission band at 610 nm. The intensity of the latter was monitored as a function of oxygen partial pressure in this study. Since the conventional ion-exchange method for Ru–Na–Y synthesis would not work for samples with Si/Al > 100, a new procedure was developed. $Ru(bpy)_3^{2+}$ was synthesized by refluxing a calcined dealuminated zeolite with $[Ru(NH_3)_5Cl]Cl_2$ in water/ CH_3CN (allowing for uptake into the zeolite as a neutral species) followed by reaction with 2,2'-bipyridyl at 200 °C.

2.5. Luminescence spectroscopy

Emission measurements were made using a Spex Fluorolog fluorimeter. The zeolite was pressed into a pellet and exposed to N_2 and O_2 . For Stern–Volmer analysis, experiments were done under the constant flow of air, nitrogen, oxygen or a 60/40 mixture of oxygen and nitrogen. For studies with dissolved gases, the zeolite was submerged in water saturated with the corresponding gas.

2.6. Thermogravimetric analysis

Thermogravimetric analysis (TGA) was performed using a Perkin–Elmer TGA 7 thermogravimetric analyzer. Weight loss from a 20–30 mg of sample was monitored as a function of temperature from 30 to 650 °C with a temperature ramp of 10 °C/min under a flow of air.

2.7. Zeolite characterization

X-ray powder diffraction (XRD) spectroscopy was performed with a Rigaku Geigerflex diffractometer using Ni-filtered Cu $K\alpha$ radiation (40 kV and 25 mA). Scanning electron microscopy (SEM) studies were performed on a JEOL JSM-820 scan-

ning electron microscope. Samples were mounted on copper pegs and coated with a thin gold film. IR studies were performed with a Bruker Instruments' IFS-66s Fourier transform IR spectrometer with a globar source, KBr beam splitter and DTGS detector. Solid-state ^{29}Si NMR were obtained with a Bruker AM 500 NMR spectrometer.

3. Results

3.1. Quenching in aqueous solutions

Fig. 1a shows the emission spectra of 1.5×10^{-4} M $Ru(bpy)_3^{2+}$ in N_2 - and O_2 -saturated water. The extent of quenching with dissolved O_2 is of the order of 70%, $I_0/I = 3.3$, where I_0 represents the emission in the presence of pure N_2 and I with O_2 . However, for $Ru(bpy)_3^{2+}$ encapsulated in zeolite Y with Si/Al = 2.5, there is no quenching by O_2 -saturated water, as shown in Fig. 1b.

3.2. Quenching of Ru–Na–Y by gas phase dry oxygen

3.2.1. Ru–Na–Y (Si/Al = 2.5)

Zeolite Y used for these studies was obtained commercially, had dimensions of the order of a micron and a Si/Al ratio of 2.5. The loading level was 1 $Ru(bpy)_3^{2+}$ per 15 supercages (Ru–Na–Y). The intrazeolitic water content (IWC) of the samples was estimated from the change in weight of a hydrated zeolite. Fig. 2 shows the thermogravimetric data. The weight loss upon complete dehydration for Na–Y was of the order of 25%, indicative of about 240 water molecules per unit cell. Various dehydration levels of Ru–Na–Y were achieved by exposing a hydrated zeolite to room air and to vacuum at varying evacuation temperatures. The samples were weighed before and after treatment, and from the decrease in weight, and the knowledge from TGA, the extent of water loss was estimated and correlated with the degree of quenching. For a sample exposed to ambient conditions, IWC was 98%, and the amount of quenching in O_2 was of the order of 6% ($I_0/I = 1.07$). For samples exposed to vacuum for 75 min at room temperature, the quenching was

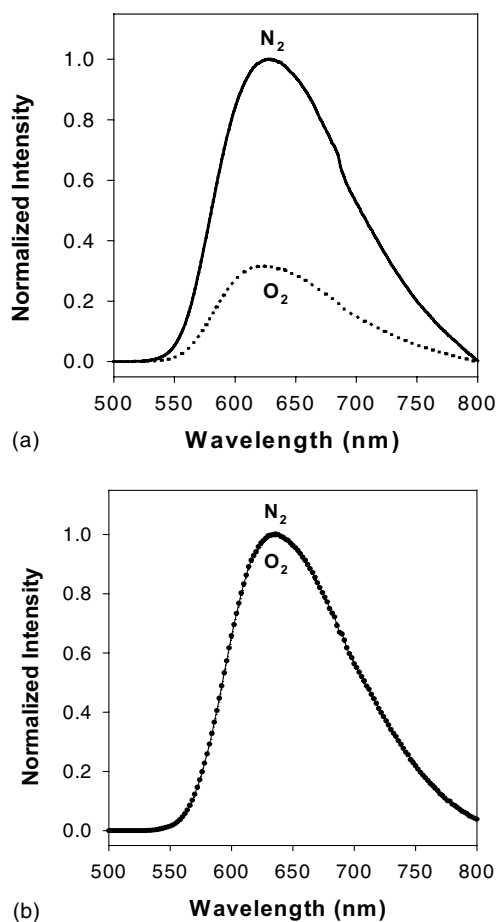


Fig. 1. Emission spectra of (a) 1.5×10^{-4} M $\text{Ru}(\text{bpy})_3^{2+}$ in N_2 (—) and O_2 (•••) saturated water, (b) $\text{Ru}(\text{bpy})_3^{2+}$ -zeolite Y in N_2 (—) and O_2 saturated water (•••).

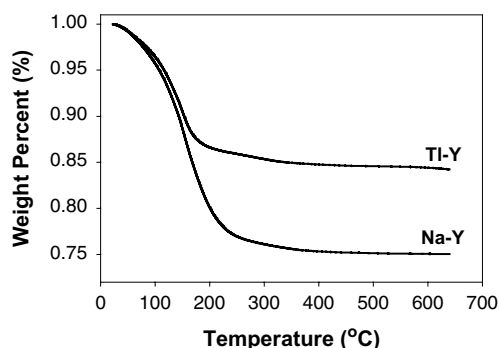


Fig. 2. TGA of hydrated zeolite Y ion exchanged with Na^+ and Tl^+ ion.

66% ($I_0/I = 3.0$), whereas IWC was 46%. For samples heated under vacuum at 250°C overnight, the quenching by O_2 was of the order of 90% ($I_0/I = 10.7$), and IWC was 0%. Table 1 lists the various samples that were examined, the extent of quenching and the water content.

The extent of quenching with different concentrations of O_2 (pure N_2 , air, 60% O_2 –40% N_2 and pure O_2) was studied and the results examined as Stern–Volmer plots, as shown in Fig. 3 for the Ru–Na–Y sample (IWC = 30%). Classically, the Stern–Volmer relationship describes the change in luminescent intensity as a function of quencher concentration in a homogeneous solution, and the I_0/I typically bears a linear relationship with the quencher concentration [12]. Demas and co-

Table 1

Comparison of the oxygen quenching of Ru–Na–Y (Si/Al = 2.5) as a function of IWC (all evacuation at 25°C unless mentioned otherwise)

Sample	Vacuum time	I_0/I	IWC ^a (%)
Hydrated Ru–Na–Y	0	1.0	100
Ambient Ru–Na–Y	0	1.07	98
Ru–Na–Y	75 min	3.0	46
Ru–Na–Y	12 h	6.9	20
Ru–Na–Y	12 h ^b	10.7	0
Nano-Ru–Na–Y	12 h	25.3	45

^a IWC = Intra zeolitic water content.

^b At 250°C , vacuum reading— 5×10^{-5} Torr.

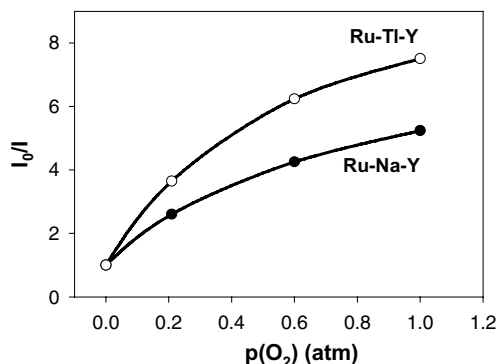


Fig. 3. Stern–Volmer plots for partially dehydrated Ru–Na–Y (Si/Al = 2.5) (IWC = 30%) and ambient exposed Ru–Tl–Y (Si/Al = 2.5) and the corresponding fits to the data using Eq. (1).

workers have modified the original form of the Stern–Volmer relationship to account for the heterogeneity of chromophoric sites in solid matrices [13]. In particular, a two-site model was developed, assuming the molecule being quenched located in two distinct environments that result in different unquenched lifetimes, as given by Eq. (1)

$$\frac{I_0}{I} = \frac{1}{\frac{f_{01}}{1 + K_{SV1}pO_2} + \frac{1 - f_{01}}{1 + K_{SV2}pO_2}} \quad (1)$$

where f_{01} and $1 - f_{01}$ are the fractional contributions of each site and K_{SV} are the corresponding Stern–Volmer constants, and pO_2 is the partial pressure of O_2 [13]. The magnitudes of f and K_{SV} provide a measure of the heterogeneity of the sites and the efficiency of the quenching of the chromophore luminescence by oxygen, respectively. Table 2 lists the f and K_{SV} values for the different samples that have been examined in this study. For the Ru–Na–Y (IWC = 30%), site I had a population of 87% with a K_{SV} of 11.5 atm⁻¹, whereas the second site with a population of 13% was poorly quenched with a K_{SV} of 0.08 atm⁻¹.

3.2.2. Ru–Tl–Y (Si/Al = 2.5)

Upon initial exposure to O_2 , the emission of Ru–Tl–Y was quenched by 67% ($I_0/I = 3$), significantly higher than Ru–Na–Y. However, as shown in Fig. 4, there is a time dependence of the extent of quenching as a function of N_2/O_2 exposure. As time progresses, there is a gradual increase in quenching and eventually, a steady state quenching of 86% ($I_0/I = 7.3$) was achieved. In the case of Ru–Na–Y, no such time dependence was observed. The TGA data in Fig. 2 shows that for Tl–Y, the weight loss upon complete dehydration is about 15% and corresponds to 192 molecules per

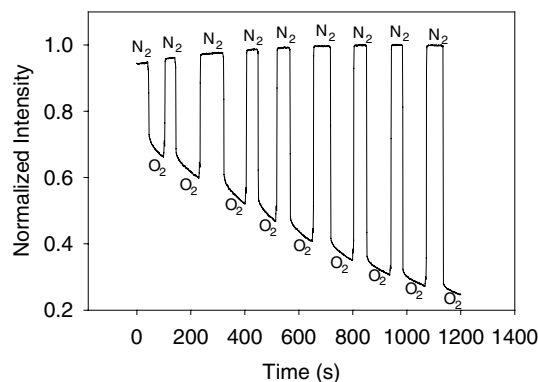


Fig. 4. Quenching profiles of ambient exposed Ru–Tl–Y (Si/Al = 2.5) in N_2/O_2 as a function of time.

unit cell [14]. Thus, as compared to Na–Y, the Tl–Y has less water in the sample. Analysis of the Stern–Volmer plots for ambient-equilibrated Ru–Tl–Y (Fig. 3) indicated that 93% of the chromophore was in a site with a K_{SV} of 14 atm⁻¹ and the molecules present in the second site with a population of 7% were not quenched at all.

3.2.3. Nanocrystalline zeolite (Si/Al = 1.7)

Nanocrystalline zeolite Y (nano-Y) was synthesized by procedures developed by Schoeman and co-workers [9]. The product was characterized by using XRD and SEM. The crystals were of the size of ~100 nm, and had well defined octahedral morphology. The Si/Al ratio of the nano-Y was found to be 1.7 by ²⁹Si NMR spectroscopy. The loading level of ruthenium complexes per supercage was the same as micron-sized Na–Y (1 Ru(bpy)₃²⁺ per 15 supercages).

TGA analysis of the micron-sized and nano-Y show that they have similar water content (data not shown) as regular Na–Y. Quenching

Table 2

Results of the two-site Stern–Volmer analysis for a series of Ru(bpy)₃²⁺-zeolite samples

Sample	f_{01}	f_{02}	K_{SV1} (atm ⁻¹)	K_{SV2} (atm ⁻¹)
Ru–Na–Y	0.87	0.13	11.5	0.08
Ru–Tl–Y	0.93	0.07	14.0	8.0×10^{-9}
Dealuminated Ru–Y (Si/Al = 9.5)	0.68	0.32	5.7	2.5×10^{-9}
Nano-Ru–Y	0.99	0.01	40.0	5.2×10^{-9}
Dealuminated nano-Ru–Y	0.69	0.31	10.5	0.47

measurements with dry O₂ showed higher sensitivity ($I_0/I = 1.44$, 30% quenching) as compared to Ru–Na–Y. Dehydration (12 h on vacuum line, no heating) of the nano-Ru–Na–Y system resulted in a remarkable increase in sensitivity ($I_0/I = 25.3$, 96% quenching). The IWC after the dehydration treatment was 45%. Fig. 5 shows the emission spectra for nano-Ru–Na–Y (IWC = 45%) in N₂, air, O₂ and a 60/40 O₂/N₂ mixture, as well as the corresponding Stern–Volmer plot. Analysis of this plot indicates that almost all of the Ru(bpy)₃²⁺ is accessible to the O₂, unlike the micron-sized Ru–Na–Y (Si/Al = 2.5) samples. K_{SV} for the dehydrated nano-Ru–Na–Y was 40 atm⁻¹, higher than all the other samples that were studied.

Ion exchange of nano-Ru–Na–Y with thallium resulted in improvements in quenching ($I_0/I = 5.0$, 80%) upon exposure to oxygen.

3.2.4. Dealuminated samples

The procedures for dealumination of the zeolite samples involved treatment with (NH₄)₂SiF₆ or SiCl₄. The extent of dealumination was monitored using IR and NMR spectroscopies. The IR band around 1000 cm⁻¹, corresponding to an asymmetric Si–Al–O stretch, is sensitive to the Si/Al ratio and shifts to higher frequencies [10]. For the (NH₄)₂SiF₆ treated sample, the band at 1005 cm⁻¹

for Si/Al = 2.5 shifted to 1085 cm⁻¹ upon dealumination. The Si/Al ratio determined by ²⁹Si NMR was found to be 9.5.

The quenching of the Ru–Na–Y (Si/Al = 9.5) sample by oxygen under ambient conditions increased compared to the Ru–Na–Y (Si/Al = 2.5), with a quenching of 38% ($I_0/I = 1.6$). Quenching measurements were also performed on dealuminated nanocrystalline zeolite Y prepared using (NH₄)₂SiF₆ treatment, and found to be 73% ($I_0/I = 3.7$). Results from fitting the emission data with Eq. (1) for dealuminated Ru–Na–Y and dealuminated nano-Ru–Na–Y is shown in Table 2. Dealumination leads to decrease in the amount of accessible Ru(bpy)₃²⁺ with only about 68% of the chromophores being accessible.

Highly dealuminated Na–Y was prepared by treatment of Na–Y with SiCl₄ to achieve framework ratio of >100. The quenching by dry O₂ was of the order of 40% ($I_0/I = 1.7$).

3.3. Quenching by hydrated O₂ and dissolved O₂

The luminescence quenching was also monitored in the presence of water saturated gas and with samples immersed in gas-saturated water. Upon exposure of the Ru–Na–Y, Ru–Ti–Y and nano-Ru–Na–Y, to water saturated O₂ or O₂ dissolved in water, there is no quenching at all ($I_0/I = 1$) (e.g. Fig. 1b). Oxygen dissolved in hexane exhibited quenching for Ru–Na–Y (Si/Al = 2.5) of the order of 25% ($I_0/I = 1.36$), indicating that hexane does not inhibit intrazeolitic oxygen transport to the same degree as water.

Dealumination of the zeolite framework (Si/Al = 9.5) proved effective in promoting oxygen quenching in wet environments, though there is a clear progression of sensitivity loss as the environment goes from dry (40%, $I_0/I = 1.7$) to water saturated O₂ (13%, $I_0/I = 1.15$) to an aqueous environment (7%, $I_0/I = 1.08$) with dissolved O₂. For the highly siliceous samples prepared by SiCl₄ treatment, the quenching with dry O₂ is about 44% ($I_0/I = 1.8$) and decreased to 23% quenching ($I_0/I = 1.3$) upon quenching by dissolved O₂ in water. Fig. 6 shows the emission profiles in N₂- and O₂-saturated water for the highly siliceous sample (Si/Al > 100) and can be contrasted with

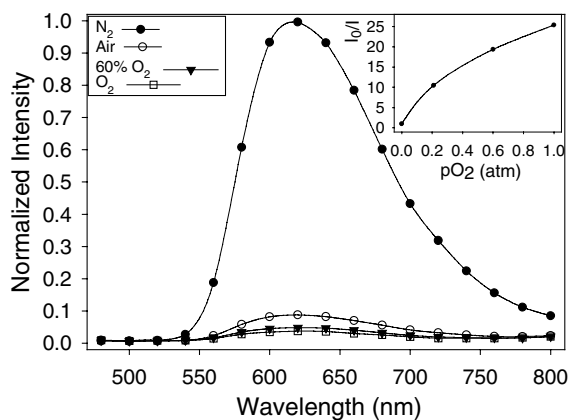


Fig. 5. Emission profiles and corresponding Stern–Volmer plot (inset) for dehydrated nanocrystalline Ru–Na–Y (IWC = 45%) in the presence of dry gases. The solid line (inset) corresponds to the fit obtained with the two-site model.

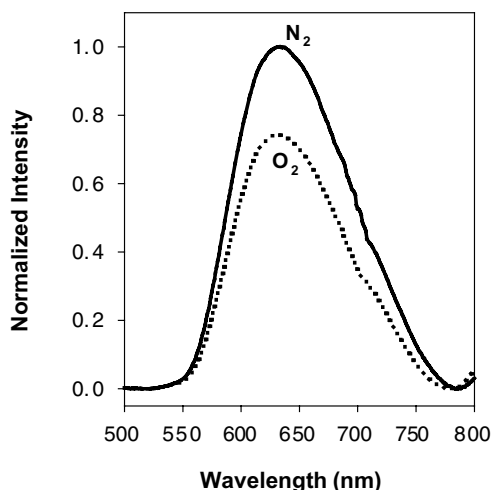


Fig. 6. Emission spectra of siliceous zeolite Y (Si/Al > 100) in N_2 and O_2 saturated water.

Fig. 1b, which shows the identical experiment for a non-dealuminated sample.

4. Discussion

Wolfbeis and co-workers were the first to report quenching of intrazeolitic $Ru(bpy)_3^{2+}$ by O_2 [8]. Their studies were done with dealuminated samples of Si/Al ratio of 4–5, made by EDTA treatment. They noted efficient quenching, but the extent of dehydration as well as dependence on crystal morphology and Si/Al ratio was not examined. In this study, we examined the O_2 transport properties in greater detail.

4.1. Oxygen transport

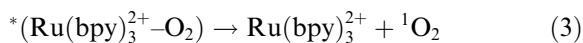
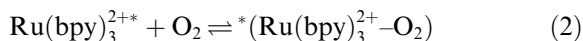
There have been a number of studies focusing on diffusion of O_2 in polymeric membranes, with the goal of optimizing optical oxygen sensors [5,15]. The efficiency of quenching has been related to the excited state lifetime of the chromophore, the solubility of oxygen in the support medium, and the quenching rate constant. Mills and co-workers have studied the quenching properties of $Ru(bpy)_3^{2+}$ in a variety of plasticizers and found that K_{SV} (which is a measure of the quenching efficiency) was inversely dependent on the viscosity

of the plasticizer [5c,15a]. It was proposed that the differences in quenching was dependent on the quenching rate constant, which increased with decreasing viscosity. Increased quenching has also been observed if plasticizers with low viscosity are incorporated in increasing amounts into a polymer, e.g. I_0/I values in pure oxygen varied from 3–20 (67–95% quenching) for a tris(4,7-diphenyl-1,10-phenanthroline)ruthenium (II), $Ru(dpp)_3^{2+}$ within cellulose acetate with varying levels of plasticizer [15b]. It is to be noted that the extent of quenching for this chromophore is considerably higher than $Ru(bpy)_3^{2+}$ in similar matrices, due to the longer lifetime of $Ru(dpp)_3^{2+}$ [15b]. For a particular chromophore, the permeability of O_2 (related to the product of diffusion coefficient and solubility) in the matrix was deemed to be the most important factor for the efficiency of quenching [15c]. In general, it has been reasoned that since the solubility of oxygen is relatively constant between different reaction media, the extent of quenching is dependent on the diffusion coefficient of oxygen.

In hydrated zeolite Y, the lifetime of the excited state of $Ru(bpy)_3^{2+}$, as well as other optical spectroscopic properties is similar to that in solution [6]. Thus, the profound differences that are observed in the O_2 quenching of $Ru(bpy)_3^{2+}$ as it is moved from an aqueous medium (70% quenching) to the aqueous medium inside the zeolite (0% quenching) must be related to the inaccessibility of the chromophore to O_2 .

4.2. Role of intrazeolitic water upon quenching

Photoexcited $Ru(bpy)_3^{2+}$ (aq) is effectively quenched by O_2 by a bimolecular process in solution [5]. The energy transfer mechanism responsible for the quenching is [16]:



where $*(Ru(bpy)_3^{2+}-O_2)$ is an exciplex formed upon collision of the two species. The extent of quenching is determined by the solubility of O_2 in water, which for a saturated solution is of the order of 9 ppm at 20 °C [17].

In the zeolite, the $\text{Ru}(\text{bpy})_3^{2+}$ is trapped in the cages and is immobile, so quenching will require migration of O_2 through the framework. This is in contrast to other solid matrices, such as silica, where collisions of gas molecules with the surface can lead to quenching [18]. For hydrated Ru–Na–Y ($\text{Si}/\text{Al} = 2.5$), the lack of quenching indicates that O_2 is either insoluble or has a very low diffusion coefficient in the aqueous interior of the zeolite. As the level of zeolite dehydration increases, quenching with O_2 gradually increases. The correlation between the extent of quenching and the number of water molecules in the supercages follows the order, no quenching with 30 water molecules, 67% quenching with 14 water molecules and 90% quenching for 0 water molecules. Thus, the role of intrazeolitic water in reducing oxygen permeability is clearly evident. The two factors that are involved include the “solubility” of O_2 in the zeolite, which is related to oxygen partial pressure ($p\text{O}_2$) by $[\text{O}_2]_{\text{zeolite}} = Kp\text{O}_2$, where K is dependent on the extent of dehydration. Second, the intrazeolitic water increases the tortuosity of the oxygen diffusion pathways.

The role of intrazeolitic water is also evident in the increased quenching of Ru–Ti–Y ($\text{Si}/\text{Al} = 2.5$) as compared to the Na–Y form. The TGA data indicate that the Ti–Y has lower water content than Na–Y zeolite. Studies on Ti^+ exchanged zeolite A and analcime have shown that intrazeolitic water is held less tightly than in Na^+/K^+ exchanged form, and that the water in the Ti^+ zeolites is more mobile [19,20]. The change in electronegativity of the zeolite can account for the difference in water content between different ion-exchanged forms, since lower electronegativity would indicate weaker interaction of the framework with water. Electronegativity of the zeolite can be computed from the Sanderson’s partial charge values with the following equations:

$$S_Z = (S_M^p S_{\text{Si}}^q S_{\text{Al}}^r S_{\text{O}}^t)^{1/(p+q+r+t)} \quad (4)$$

$$\delta = (S_Z - S_X)/(2.08S_X^{1/2}) \quad (5)$$

where S_M , S_{Si} , S_{Al} , and S_{O} are the Sanderson electronegativities for the cation, silicon, aluminum and oxygen respectively; p , q , r , and t are the number of the corresponding element in a unit cell;

and δ is the average partial charge for element X within the zeolitic structure [21,22]. Calculations of these partial charges show lower values for Ti^+ (0.83) as compared to the Na^+ (1.30), suggesting that in the Ti^+ sample, there should be a weaker electrostatic attraction for dipolar water [23]. Charge on framework oxygen atoms was found to be -0.27 for Na–Y, and -0.24 for Ti–Y, indicating that the framework is less polar upon Ti^+ exchange. Thus, the increased quenching in the Ru–Ti–Y is proposed to arise from the lower water content in the zeolite and ready loss of this water even under ambient conditions, in flowing gas.

The picture that emerges from the discussion above is that intrazeolitic water blocks oxygen transport. Partial removal of the water allows transport. We propose that in a fully hydrated zeolite, O_2 does not dissolve in the intrazeolitic volume, presumably because of the packing of the water molecules and the network structure. With increasing dehydration, oxygen solubility and diffusion constant increases leading to increased quenching. In hexane filled zeolite, intrazeolitic oxygen diffusion is enhanced as compared to water. Previous studies have shown that organics have a smaller effect than water on restricting intrazeolitic mobility e.g., self-diffusion of paraffins in Na–X exhibited a decrease in mobility of three orders of magnitude upon the addition of water, whereas the effect of additional hydrocarbon molecules was minimal [24]. It was concluded that the influence of water could not be explained by a reduction in molecular free volume, but that cation–water complexes posed a barrier to transport between supercages. Scaiano and co-workers reported that the mobility of pyrene within Na–Y was reduced by intrazeolitic water considerably more so than with hexane [25]. Iu and Thomas have also studied the photophysics of intrazeolitic pyrene and noted a decrease in oxygen quenching efficiency upon addition of water [26]. They concluded that the diffusion of O_2 was blocked by the coadsorbed water that formed a rigid structure. A study on anthracene triplet self-quenching as a probe for intrazeolitic mobility [27] found that though small amounts of water (~ 8 molecules per supercage) promoted intrazeolitic mobility since this water is held close to the framework by

cations, allowing for motion of the anthracene through the supercage. The motion becomes significantly hindered at higher levels of hydration (~26 molecules per supercage), due to water blocking the windows between supercages.

4.3. Heterogeneity of $\text{Ru}(\text{bpy})_3^{2+}$ within zeolites

The Stern–Volmer curves for quenching by gas phase O_2 for all zeolite samples were non-linear and typical of other heterogeneous systems. Results from the Stern–Volmer analyses provide insight into the nature of heterogeneity within the zeolite lattice. It has been proposed that non-linearity arises from the inhomogeneity of the environments around the Ru complex, and the two-site model has accounted well for the non-linearity [5,13,15,28]. The two chromophore environments in the zeolite have different degrees of quenching, a site with relatively high K_{SV} values (site I) and the second site with K_{SV} values that are smaller, and in most cases approach zero (site II). Site II is indicative of locations where intrazeolitic $\text{Ru}(\text{bpy})_3^{2+}$ is inaccessible to oxygen. For the dehydrated Na–Y and ambient Tl–Y samples the fraction of site II is ~10%, whereas, for nanocrystalline zeolites, only 1% of the ruthenium complexes are in site II.

The zeolite, by virtue of its well defined crystalline structure provides uniformity in not only the distribution of supercages but also their environments, and thus ideally all $\text{Ru}(\text{bpy})_3^{2+}$ should be present in only a single site. This can be contrasted with other matrices, such as silica and alumina, where there is a heterogeneous distribution of surface sites. Also, by maintaining a low loading, interactions between the $\text{Ru}(\text{bpy})_3^{2+}$ molecules in the supercages are minimized. We propose that the heterogeneity of sites in zeolites arises from internal crystal defects, which decrease/block O_2 permeability through regions of the crystal. These defects are produced both during synthesis of the zeolite and the synthesis of $\text{Ru}(\text{bpy})_3^{2+}$. We have noted earlier that significant fractions of $\text{Ru}(\text{bpy})_3^{2+}$ synthesized within zeolite X can remain inaccessible to quenching molecules, because of the decomposition of the zeolite during chromophore synthesis [7c]. This process is alleviated in higher Si/Al ratio zeolites, but can still occur. The

nanozeolites have fewer defects than the commercially obtained micron-sized zeolite, though powder diffraction indicates that both materials are crystalline. The hypothesis of defects inhibiting oxygen diffusion is supported by the dealuminated samples. It is known that the process of dealumination leads to creation of defects, including extraframework aluminum species [29]. Thus upon dealumination by $(\text{NH}_4)_2\text{SiF}_6$, the amount of inaccessible $\text{Ru}(\text{bpy})_3^{2+}$ increases significantly to about 30% for both the micron and nanozeolites. The K_{SV} of the accessible $\text{Ru}(\text{bpy})_3^{2+}$ also decreases since the diffusion of O_2 has to follow more tortuous routes because of the defects.

4.4. Efficiency of quenching by gas phase O_2

The other difference observed between the different zeolite samples is the magnitude of K_{SV} . The extent of quenching observed in the nanocrystalline zeolite for $\text{Ru}(\text{bpy})_3^{2+}$ is higher than any matrix reported to date ($I_0/I = 25.3$) by almost an order of magnitude. Even for the micron-sized zeolite Y, though the extent of quenching for a completely dehydrated sample is a factor of 4 lower than in naocrystalline zeolite, the magnitude of quenching is still very high. Table 3 compares the I_0/I values for $\text{Ru}(\text{bpy})_3^{2+}$ quenching by O_2 in different matrices and it is clear that zeolite encapsulation has a profound effect on the quenching. Zeolites possess remarkable catalytic properties and considerable discussion has centered on the reasons for their catalytic processes [30]. Freeman has proposed that the marked accelerating effect of the zeolite on reactions within its cages arises because in the molecular sized cavities, the mean free path for collisions is very small [31]. This can also be manifested as what Fraissard described as a “pressure effect”, in which the confinement of molecules within the zeolite leads to higher probability of collision between reactants, thereby enhancing the reaction rate [32]. We propose that the high K_{SV} 's observed in the zeolite has its origin in the confinement of the O_2 molecules, that leads to enhanced quenching. Fraissard has calculated that for one Xe atom in a supercage, the number of collisions with the wall is increased by a factor of 100 as compared to a planar surface, for

Table 3
Quenching of oxygen by $\text{Ru}(\text{bpy})_3^{2+}$ by O_2 (1 atm.) in different matrices

$\text{Ru}(\text{bpy})_3^{2+}$ matrix	I_0/I	Reference
$\text{Ru}(\text{bpy})_3^{2+}$ in RTV 118	2.52	[13]
$\text{Ru}(\text{bpy})_3^{2+}(\text{ClO}_4^-)_2$ in silicone rubber	2.58	[13]
$\text{Ru}(\text{bpy})_3^{2+}\text{Cl}_2$ in silicagel-based Silicone elastosil E4 membrane	4.16	[8]
$\text{Ru}(\text{bpy})_3^{2+}\text{Cl}_2$ in zeolite with Silicone elastosil E4 membrane	3.50	[8]
$\text{Ru}(\text{bpy})_3^{2+}$ in Cab–O–Sil disks	5.20	[5b]
$\text{Ru}(\text{bpy})_3^{2+}(\text{Ph}_4\text{B}^-)_2$ in PMMA films with plasticizers TPP (tripropyl phosphate)	2.77	[5c]
$\text{Ru}(\text{bpy})_3^{2+}\text{Cl}_2$ in TEOS based sol–gel films	1.26	[5d]
$\text{Ru}(\text{bpy})_3^{2+}$ in kieselgel-type membrane	4.48	[5e]
$\text{Ru}(\text{bpy})_3^{2+}\text{Cl}_2$ in TEOS based sol–gel films	2.0	[5f]
$\text{Ru}(\text{bpy})_3^{2+}\text{Cl}_2$ adsorbed on silica gel	3.05	[5g]
Dehydrated Ru–Na–Y	10.7	This work
Dehydrated Ru–Na–nanocrystalline Y	25.3	This work

comparable pressures of Xe [32]. Such an increase in collisions with O_2 in the supercages should lead to enhanced quenching. Planar surfaces can also promote quenching due to adsorption effects that lead to increased interaction time of probe and quencher, though the effects are not as marked as observed from confinement [18]. The higher quenching for the nanocrystalline zeolites arises from their higher internal crystallinity, which ensures facile diffusion of the O_2 molecules.

4.5. Hydrophobicity of zeolite and quenching

The dealuminated sample with $\text{Si}/\text{Al} = 9.5$ made by treating $\text{Ru}(\text{bpy})_3^{2+}\text{–Na–Y}$ ($\text{Si}/\text{Al} = 2.5$) with $(\text{NH}_4)_2\text{SiF}_6$ led to increased sensitivity to oxygen quenching in aqueous solution as compared to frameworks with Si/Al of 2.5. Increasing the framework Si/Al above 100 by treatment with SiCl_4 improved the quenching further. Thus, with increasing dealumination, the quenching by O_2 dissolved in water is improving. With dealumination, the amount of water adsorbed by the zeolite decreases [33]. Therefore, the O_2 that is transferred from H_2O to the zeolite can migrate unimpeded through the cages. The adsorption capacity for O_2 from an aqueous phase into hydrophobic zeolites has not been measured. For hydrophobic chlorinated organic compounds, it has been determined that transfer from an aqueous phase into siliceous zeolites is facile [33a]. Thus, for quenching by dissolved oxygen, it is

necessary to insure that water inside the zeolite cages is absent and can be accomplished with hydrophobic zeolites.

5. Conclusions

The ability of water to block oxygen diffusion within zeolites is due to the rigid structure of intrazeolitic water that cannot be easily disrupted. Partial dehydration is necessary for oxygen entry and migration within the zeolite. For Tl–Y, water loss from the zeolite is promoted by the lowering of the overall polarity of the zeolitic environment. The quenching of $\text{Ru}(\text{bpy})_3^{2+}$ within dehydrated nanocrystalline zeolite Y is the best reported to date considering all matrices and is proposed to arise from the cage effects that lead to enhanced collisions. Based on Stern–Volmer analysis of the quenching data, two sites with only one of them accessible to O_2 were found. The relative ratio of these two sites depended on the defects in the zeolite that were incorporated during synthesis. The nanocrystalline zeolite was found to be more defect free than commercially obtained micron-sized crystallites, and led to more efficient quenching. Zeolites with low Si/Al ratios were too hydrophilic for quenching by O_2 in dissolved water. Dealumination was necessary to reduce the zeolite affinity for water. The use of highly dealuminated, hydrophobic zeolites allowed for efficient quenching by dissolved oxygen.

Acknowledgements

We acknowledge support from NSF (EEC 9872531), NASA and The Ohio State University Graduate School for a fellowship to MAC.

References

- [1] A. Galarneau, F.D. Renzo, F. Fajula, J. Védérine (Eds.), *Zeolites and Mesoporous Materials at the Dawn of the 21st Century, Studies in Surface Science and Catalysis*, vol. 135, Elsevier, Amsterdam, 2001.
- [2] J. Kärger, D.M. Ruthven, *Diffusion in Zeolites*, John Wiley & Sons, New York, 1992.
- [3] (a) M.F.N. Post, J. van Amstel, H.W. Kouwenhoven, in: D. Olson, A. Bisio (Eds.), *Diffusion and Catalytic Reaction of 2,2-Dimethylbutane in ZSM-5 Zeolite*, Butterworths, Guilford, Surrey, UK, 1983, p. 517;
(b) J. Caro, S. Hocevar, J. Kärger, L. Riekert, *Zeolites* 6 (1986) 213;
(c) J. Kärger, H. Pfeifer, *Zeolites* 7 (1987) 90;
(d) S. Vasenkov, W. Bohlmann, P. Galvosas, O. Geier, H. Liu, J. Kärger, *J. Phys. Chem. B* 105 (2001) 5922;
(e) N.K. Moroz, E.V. Kholopov, I.A. Belitsky, B.A. Fursenko, *Micropor. Mesopor. Mater.* 42 (2001) 113.
- [4] A.S. Vaidyalngam, M.A. Coutant, P.K. Dutta, in: V. Balzani (Ed.), *Electron Transfer in Chemistry*, vol. 4, Wiley-VCH, Weinheim, Germany, 2001, p. 412.
- [5] (a) J.N. Demas, B.A. DeGraff, P.B. Coleman, *Anal. Chem.* (1999) 793A;
(b) E.R. Carraway, J.N. Demas, B.A. DeGraff, *Langmuir* 7 (1991) 2998;
(c) A. Mills, M.D. Thomas, *Analyst* 123 (1998) 1135;
(d) M. Ahmad, N. Mohammad, J. Abdullah, *J. Non-Cryst. Solids* 290 (2001) 86;
(e) O.S. Wolfbeis, M.J.P. Leiner, H.E. Posch, *Mikrochim. Acta* 3 (1986) 359;
(f) B.D. MacCraith, C.M. McDonagh, G. O'Keeffe, E.T. Keyes, J.G. Vos, B. O'Kelly, J.F. McGilp, *Analyst* 118 (1993) 385;
(g) P. Hartmann, M.J.P. Leiner, M.E. Lippitsch, *Sens. Actuators B* 29 (1995) 251;
(h) H.N. McMurray, P. Douglas, C. Busa, M.S. Garley, *J. Photochem. Photobiol. A: Chem.* 80 (1994) 283.
- [6] (a) W. DeWilde, G. Peeters, J.H. Lunsford, *J. Phys. Chem.* 84 (1980) 2306;
(b) K. Maruszewski, D.P. Strommen, J.R. Kincaid, *J. Am. Chem. Soc.* 115 (1993) 8345;
(c) M. Sykora, J.R. Kincaid, P.K. Dutta, N.B. Castagnola, *J. Phys. Chem. B* 103 (1999) 309;
(d) M.A. Coutant, T. Le, N.B. Castagnola, P.K. Dutta, *J. Phys. Chem. B* 104 (2000) 10783;
(e) A. Vaidyalngam, P.K. Dutta, *Anal. Chem.* 72 (2000) 5219.
- [7] (a) M. Vitale, N.B. Castagnola, N.J. Ortins, J.A. Brooke, A. Vaidyalngam, P.K. Dutta, *J. Phys. Chem. B* 103 (1999) 2408;
(b) N.B. Castagnola, P.K. Dutta, *Stud. Surf. Sci. Catal.* 135 (2001) 4508;
(c) N.B. Castagnola, P.K. Dutta, *J. Phys. Chem. B* 105 (2001) 1537.
- [8] B. Meier, T. Werner, I. Klimant, O.S. Wolfbeis, *Sens. Actuators B* 29 (1995) 240.
- [9] (a) J.E. Otterstedt, P.J. Sterte, B.J. Schoeman, *International Patent*, WO 94/05597, 1994;
(b) B.J. Schoeman, J. Sterte, J.E. Otterstedt, *Zeolites* 14 (1994) 110.
- [10] G.W. Skeels, D.W. Breck, in: A. Bisio (Ed.), *Proceedings of the Sixth International Zeolite Conference*, Butterworth and Company, Reno, USA, 1984, p. 87.
- [11] M.W. Anderson, J. Klinowski, *J. Chem. Soc., Faraday Trans. I* 82 (1986) 1449.
- [12] N.J. Turro, *Modern Molecular Photochemistry*, The Benjamin/Cummings Publishing Company, Inc., Menlo Park, CA, 1978.
- [13] E.R. Carraway, J.N. Demas, B.A. DeGraff, J.R. Bacon, *Anal. Chem.* 63 (1991) 337.
- [14] The composition of Tl–Y was taken from: R.M. Barrer, J.A. Davies, L.V.C. Rees, *J. Inorg. Nucl. Chem.* 30 (1968) 3333.
- [15] (a) A. Mills, *Sens. Actuators B* 51 (1998) 60;
(b) A. Mills, F.C. Williams, *Thin Solid Films* 306 (1997) 163;
(c) X. Lu, M.A. Winnik, *Chem. Mater.* 13 (2001) 3449.
- [16] J.N. Demas, E.W. Harris, R.P. McBride, *J. Am. Chem. Soc.* 99 (1977) 3547.
- [17] M.L. Hitchman, *Chemical Analysis*, in: *Measurement of Dissolved Oxygen*, vol. 49, John Wiley & Sons, New York, 1978.
- [18] R. Krasnansky, K. Koike, J.K. Thomas, *J. Phys. Chem.* 94 (1990) 4521.
- [19] M. Nitta, K. Ogawa, K. Aomura, *J. Chem. Soc., Faraday Trans. I* 72 (1976) 2893.
- [20] A. Dyer, A.M. Yusof, *Zeolites* 9 (1989) 129.
- [21] (a) W. Mortier, *J. Catal.* 55 (1978) 138;
(b) R. Heidler, G.O.A. Janssens, W.J. Mortier, R.A. Schoonheydt, *J. Phys. Chem.* 100 (1996) 19728.
- [22] Y.S. Park, S.Y. Um, K.B. Yoon, *J. Am. Chem. Soc.* 121 (1999) 3193.
- [23] H.S. Frank, W.-Y. Wen, *Discuss. Faraday Soc.* 82 (1957) 133.
- [24] A. Germanus, J. Kärger, H. Pfeifer, *Zeolites* 4 (1984) 188.
- [25] F.L. Cozens, M. Regimbald, H. Garcia, J.C. Scaiano, *J. Phys. Chem.* 100 (1996) 18165.
- [26] K.-K. Iu, J.K. Thomas, *Langmuir* 6 (1990) 471.
- [27] S. Hashimoto, T. Miyashita, M. Hagiri, *J. Phys. Chem. B* 103 (1999) 9149.
- [28] (a) I. Klimant, O.S. Wolfbeis, *Anal. Chem.* 67 (1995) 3160;
(b) M.M.F. Choi, D. Xiao, *Anal. Chim. Acta* 403 (2000) 57.

- [29] (a) R.A. Beyerlein, G.B. McVicker, *Stud. Surf. Sci. Catal.* 134 (2001) 3;
(b) G.J. Ray, A.G. Nerheim, J.A. Donohue, *Zeolites* 8 (1988) 458.
- [30] P.B. Weisz, *Pure Appl. Chem.* 52 (1980) 2091.
- [31] M.P. Freeman, *J. Colloid Interface Sci.* 37 (1971) 760.
- [32] J. Fraissard, *Stud. Surf. Sci. Catal.* 5 (1980) 343.
- [33] (a) A. Giaya, R.W. Thompson, R. Denkwicz Jr., *Micropor. Mesopor. Mater.* 40 (2000) 205;
(b) D.H. Olson, W.O. Haag, W.S. Borghard, *Micropor. Mesopor. Mater.* 35–36 (2000) 435.